Journal of Engineering Mathematics **43:** 201–227, 2002.

The mathematical modelling of capillary drawing for holey fibre manufacture

A.D. FITT[1], K. FURUSAWA[2], T.M. MONRO[2], C.P. PLEASE[1] and D.J. RICHARDSON[2]
[1]*Faculty of Mathematical Studies, University of Southampton, Southampton SO17 1BJ, UK*
[2]*Optoelectronics Research Centre, University of Southampton, Southampton SO17 1BJ, UK*

Received 30 October 2001; accepted in revised form 6 May 2002

Abstract. Microstructured optical fibres (*i.e.* fibres that contain holes) have assumed a high profile in recent years, and given rise to many novel optical devices. The problem of manufacturing such fibres by heating and then drawing a preform is considered for the particularly simple case of annular capillaries. A fluid-mechanics model is constructed using asymptotic analysis based on the small aspect ratio of the capillary. The leading-order equations are then examined in a number of asymptotic limits, many of which give valuable practical information about the control parameters that influence the drawing process. Finally, some comparisons with experiment are performed. For a limited set of experiments where the internal hole is pressurised, the theoretical predictions give qualitatively accurate results. For a much more detailed set of experiments carried out with a high-grade silica glass where no hole pressurisation is used, the relevant asymptotic solution to the governing equations is shown to give predictions that agree remarkably well with experiment.

Key words: asymptotic analysis, extensional flow, holey fibres, optical-fibre manufacture, slow viscous flow

1. Introduction

In this study, we discuss models relevant to the drawing of optical fibres that contain holes. Our motivation is the existence of a new and important class of optical fibres that has recently achieved increased prominence: the microstructured fibre. The transverse profile of a microstructured fibre typically contains an array of air holes that run for the whole length of the fibre. Such optical fibres have become known as "holey fibres". The basic physical principles that underlie holey fibres are no different from those that apply to solid fibres: light is guided along the fibre because of the effective difference in refractive index between the cladding, which is laced with air holes, and the solid core.

Unlike conventional optical fibres, holey fibres can be manufactured from a single material (often pure silica is used). Two examples of typical holey fibres, manufactured at the University of Southampton, are shown in Figure 1. Why should there be such interest in fibres of this type? The answer lies in the fact that it is possible (in particular when the structure scale of the holes is small) to arrange that the effective refractive-index contrast of a holey fibre is a strong function of the wavelength of the light being guided within the fibre. This allows the construction of fibres that possess a host of highly unusual and tailorable optical properties (see, for example [1–4]). In particular, holey fibres with small holes can be "endlessly single mode", so that only a single mode is transmitted regardless of wavelength. In addition, such fibres can have mode areas ranging over as many as three orders of magnitude. Large mode areas allow high optical power to be transmitted with few nonlinear effects (which is ideal for long-range transmission) while small mode areas allow nonlinear effects to be achieved at

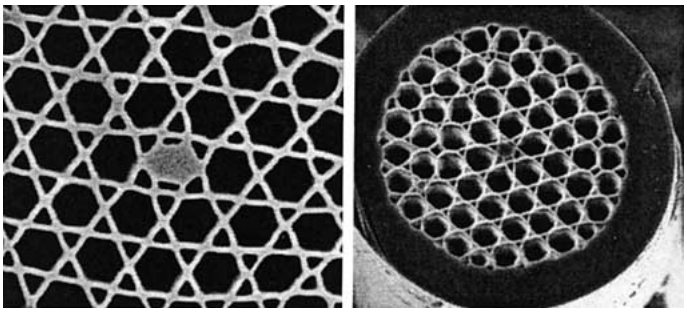

Figure 1. Two typical silica holey fibres. The fibres on the left and right have core diameters of approximately 2·5 μm and 5 μm, respectively.

low power (useful, for example, in optical switching devices). Finally, holey fibres can display anomalous dispersion throughout the visible spectrum, which allows for the possibility of soliton formation in this wavelength range, something not possible in conventional single-mode fibres.

As far as applications are concerned, the presence of air holes in holey fibres allows a vast new range of potential applications for optical fibres. These range from novel nonlinear devices to fibres that are capable of high-power delivery, and from fibres that may be used for dispersion compensation or flattening for WDM (wavelength division multiplexing) telecommunications systems to fibres that are capable of evanescent field sensing.

Other types of microstructured fibres are becoming increasingly important. Photonic bandgap fibres guide light by making use of the photonic bandgaps that may occur in a periodic structure (see, for instance [5]). Atom guiding fibres (see, for example, [6]) typically contain four holes into which platinum or gold electrodes are inserted. When a current is passed along these wires, a magnetic field is created that may be used to guide single atoms down the central hole. Atomic transport and deposition, and a number of other novel processes are thus possible.

The huge range of applications described above render it imperative that holey fibres may be manufactured in an efficient and accurate manner. Essentially, all optical fibres are produced by heating and then drawing a macroscopic preform (whose diameter is typically a few centimetres) down into fibre form (125 μm) using a conventional fibre-drawing tower. The required preforms for microstructured fibres may be manufactured in a variety of ways, and the two most common approaches are described briefly here. One method involves stacking small capillaries (which are fabricated from larger capillaries by "caning" using a fibre drawing tower) around a solid rod, which ultimately forms the fibre core. This approach is generally preferred when large air holes are required in the final fibre structure. Alternatively, the required arrangement of holes can be drilled directly in a solid glass blank. This is effective when only a few well-separated holes are required, as, for example, in the case of the atom-guiding fibres described above.

Whichever manufacturing method is used to produce a preform, the geometry of the final fibre may be significantly influenced by controlling parameters in the drawing process such as the furnace temperature, the feed speed and the draw speed. Obviously, when high temperatures or low draw speeds are used, the air holes in the cladding tend to reduce in size, and may even collapse completely because of the effects of surface tension. For some types of fibre where small holes are required, partial collapse may be exploited to draw the required

holey fibre from a readily-manufactured preform. Holes with small diameters relative to their separation distances (as required, for example, in endlessly single mode fibres) are very hard to produce by any other means. Conversely, for fibres with small mode areas or full photonic band gaps, relatively large holes are required and hole collapse should be minimised. Under some circumstances, the collapse process may be exploited to tune the final size of the air holes. One possible proposed method to control hole collapse is to pressurise the air in the holes. If such collapse control can be perfected, then there are important consequences for commercial holey-fibre manufacture, as a range of fibres with dramatically different optical properties may be made from a single preform.

The chief purpose of a mainly theoretical study such as this one is to try to quantify the parametric dependence of the drawing process on quantities such as draw and feed speed, temperature, viscosity, gravity, surface tension and hole pressurisation and thus to indicate what might be feasible as controlling mechanisms for holey-fibre fabrication. The most labour-intensive (and expensive) part of fibre manufacture is the creation of the preform; being able to control the drawing process to such an extent so as to allow different end products to be pulled from a single preform is thus extremely attractive.

Previous theoretical predictive studies of fibre drawing grew for the most part from theory that had already been developed for the textile industry to model the spinning of molten thread-lines (see, for example [7–10]). This general methodology was then adapted to steady optical-fibre drawing (see, for example [11–13]). Much of the literature concerns fibre-drawing models that are essentially small perturbations about a state of steady unidirectional extensional flow, and this is broadly the approach that we follow in this study. Various authors have examined the additional influences of heat transfer [14], surface tension [15], weak unsteadiness [8] and inertia [9]. The effects of both gravity and inertia were included in a general theory of slender viscous fibres of arbitrary cross section [16]. From a manufacturing point of view, the worst thing that can happen in a fabrication plant is that the fibre fractures. Fibre breakage was studied in [17], using an asymptotic model essentially similar to [15], showing that, if the fibre material is assumed to be a Newtonian viscous fluid, then, unless the initial conditions possess certain singularities, the cross-sectional area cannot be made to vanish in finite time.

The progress that can be made using analytical methods is necessarily limited, and a number of purely numerical studies of optical-fibre drawing have also taken place (see, for example [18–20]). The drawing of thin-walled viscous capillaries was modelled in [21] and [21] (see also [23]), and [24] included some basic estimates of the strength of hollow glass fibres for use in reinforced plastics.

Apart from these specific studies, however, no detailed theory has yet been proposed for fibres that have a cross-section containing holes. Evidently the theory of fibres that contain a large number of arbitrarily-arranged holes is likely to be extremely involved, and we do not attempt this here. Rather, as a first step towards understanding holey-fibre drawing, we seek to model the drawing of a capillary. The capillary caning problem is of direct relevance to holey-fibre manufacture because large-scale capillaries are caned prior to the production of a stacked holey-fibre preform. It also provides a useful indication about the degree of structure retention that might be expected to apply to a more complex (multi-holed) structure for given drawing conditions.

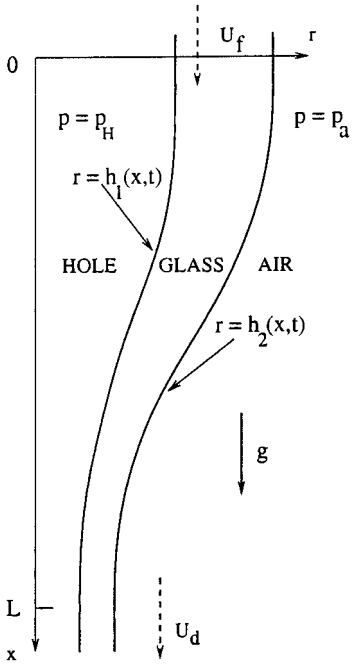

Figure 2. Schematic diagram and nomenclature for capillary.

2. Mathematical modelling

To develop a mathematical model for the process of capillary drawing that is capable of including the effects of internal hole pressurisation, surface tension and all of the other effects that we wish to analyse, we begin from the Navier-Stokes and convection-diffusion equations

$$\rho(u_t + uu_x + wu_r) = -p_x + \frac{1}{r}(\mu r u_r)_r + (2\mu u_x)_x + \frac{1}{r}(\mu r w_x)_r + \rho g, \tag{1}$$

$$\rho(w_t + uw_x + ww_r) = -p_r + \mu\left(\frac{1}{r}(rw)_r\right)_r + (\mu w_x)_x + \mu_x u_r + 2\mu_r w_r, \tag{2}$$

$$u_x + \frac{1}{r}(rw)_r = 0, \tag{3}$$

$$\rho c_p(T_t + uT_x + wT_r) = (kT_x)_x + \frac{1}{r}(krT_r)_r + \sigma\alpha(T_a^4 - T^4). \tag{4}$$

In (1)–(4), derivatives are denoted by subscripts, t denotes time, x measures the distance along the axis of a capillary, and r denotes distance normal to it. The flow has been assumed to be axisymmetric, and therefore independent of the azimuthal angle θ. The velocity $\boldsymbol{q}$ of the molten glass is denoted by $\boldsymbol{q} = u\boldsymbol{e}_x + w\boldsymbol{e}_r$ where $\boldsymbol{e}_x$ and $\boldsymbol{e}_r$ are unit vectors in the x and r directions, respectively. A schematic diagram of the geometry of the capillary is shown in Figure 2.

The pressure is denoted by p, g is the acceleration due to gravity, and density, dynamic viscosity, surface tension, thermal conductivity and specific heat are denoted by ρ, μ, γ, k and c_p, respectively. The glass temperature is denoted by T, the ambient temperature in the

furnace by T_a, σ is the Stefan-Boltzmann constant and α is a material constant that involves the emissivity of the fibre.

Regarding the modelling involved in (1)–(4), the first three equations are standard, provided that we agree that molten glass may be treated as a linear incompressible fluid. The energy-conservation equation (4) requires some further discussion. We have chosen to take a simple point of view, namely that diffusive and convective heat transfer in the fibre are accounted for as normal, viscous dissipation is ignored, and that the fibre, being optically thin, absorbs radiation directly from the surrounding furnace and re-radiates heat back to the furnace. Many other similar models have been discussed in the literature (see, for example, [25], [26], [18], [10] and [20]). We note that more detailed modelling may be appropriate, particularly in accounting more carefully for the radiation field within the fibre and the resulting body heating. The boundary conditions for the equations also have an important role to play; these will be discussed fully below.

Some discussion concerning the variation of the physical constants with temperature is also apposite. In reality, each of ρ, k, γ, c_p, μ and α varies with temperature. In practice, however, though the viscosity of the glass may vary by orders of magnitude over a relatively modest temperature range, the other parameters are only weak functions of T (see, for example [25]). For the remainder of this study we therefore assume that μ alone is a function of temperature.

As shown in Figure 2, we denote the inner and outer radii of the capillary by $r = h_1(x, t)$ and $r = h_2(x, t)$, respectively. The equations (1)–(3) thus apply in the region $h_1 \leq r \leq h_2$, and must be solved subject to suitable boundary and initial conditions, which will be considered presently. The feed and draw speeds are denoted by U_f and U_d, respectively, the ambient pressure in the air surrounding the fibre is denoted by p_a and the pressure in the hole by p_H.

It is now appropriate to non-dimensionalise (1)–(4) to take advantage of the small parameters that are present in the problem. We set $x = L\bar{x}$, $r = h\bar{r}$, $t = (L/U)\bar{t}$, $h_1 = h\bar{h}_1$, $h_2 = h\bar{h}_2$, $\mu = \mu_0\bar{\mu}$, $p = (\mu_0 UL/h^2)\bar{p}$, $u = U\bar{u}$, $w = (hU/L)\bar{w}$, $T_a = T_R\bar{T}_a$ and $T = T_R\bar{T}$ where an overbar denotes a non-dimensional quantity and L denotes a typical hot-zone length in the fibre-drawing furnace. Here h denotes a typical drawn capillary size, U denotes a typical draw speed and μ_0 and T_R denote a typical glass viscosity and fibre reference temperature, respectively. The equations now become

$$\epsilon^2 \,\mathrm{Re}[\bar{u}_{\bar{t}} + \bar{u}\bar{u}_{\bar{x}} + \bar{w}\bar{u}_{\bar{r}}] = -\bar{p}_{\bar{x}} + \epsilon^2(2\bar{\mu}\bar{u}_{\bar{x}})_{\bar{x}} + \frac{1}{\bar{r}}(\bar{\mu}\bar{r}\bar{u}_{\bar{r}})_{\bar{r}} + \frac{\epsilon^2}{\bar{r}}(\bar{\mu}\bar{r}\bar{w}_{\bar{x}})_{\bar{r}} + \frac{\epsilon^2 \mathrm{Re}}{Fr},$$

$$\epsilon^2 \,\mathrm{Re}[\bar{w}_{\bar{t}} + \bar{u}\bar{w}_{\bar{x}} + \bar{w}\bar{w}_{\bar{r}}] = -\frac{\bar{p}_{\bar{r}}}{\epsilon^2} + \epsilon^2(\bar{\mu}\bar{w}_{\bar{x}})_{\bar{x}} + \bar{\mu}\left(\frac{1}{\bar{r}}(\bar{r}\bar{w})_{\bar{r}}\right)_{\bar{r}} + \bar{\mu}_{\bar{x}}\bar{u}_{\bar{r}} + 2\bar{\mu}_{\bar{r}}\bar{w}_{\bar{r}},$$

$$\bar{u}_{\bar{x}} + \frac{1}{\bar{r}}(\bar{r}\bar{w})_{\bar{r}} = 0,$$

$$\bar{T}_{\bar{t}} + \bar{u}\bar{T}_{\bar{x}} + \bar{w}\bar{T}_{\bar{r}} = \frac{1}{\mathrm{Pr}\,\mathrm{Re}}(\bar{T}_{\bar{x}})_{\bar{x}} + \frac{1}{\bar{r}\epsilon^2 \mathrm{Pr}\,\mathrm{Re}}(\bar{r}\bar{T}_{\bar{r}})_{\bar{r}} + \Gamma(\bar{T}_a^4 - \bar{T}^4),$$

where the key non-dimensional parameters in the problem are given by

$$\epsilon = \frac{h}{L}, \quad \mathrm{Re} = \frac{LU\rho}{\mu_0}, \quad \mathrm{Fr} = \frac{U^2}{gL}, \quad \mathrm{Pr} = \frac{\mu_0 c_p}{k},$$

and

$$\Gamma = \frac{L\sigma\alpha T_R^3}{\rho c_p U}.$$

A full consideration of the relative sizes of each of the non-dimensional parameters above would require us to consider specific drawing scenarios, and we wish to propose as general a model as possible. We therefore simply note at this stage that in all drawing configurations $h \ll L$ (the largest values of ϵ tend to occur for capillaries, where L is of order cm and h of order mm. For optical fibres ϵ is much smaller). We shall therefore assume henceforth that the small parameter in the problem is $\epsilon \ll 1$. The leading-order equations in ϵ are now satisfied by the obvious *ansatz*

$$\bar{u} = \bar{u}_0(\bar{x}, \bar{t}) + \epsilon^2 \bar{u}_1(\bar{x}, \bar{r}, \bar{t}) + \dots ,$$
$$\bar{w} = \bar{w}_0(\bar{x}, \bar{r}, \bar{t}) + \epsilon^2 \bar{w}_1(\bar{x}, \bar{r}, \bar{t}) + \dots ,$$
$$\bar{p} = \bar{p}_a + \epsilon^2 \bar{P}(\bar{x}, \bar{r}, \bar{t}) + \dots ,$$
$$\bar{T} = \bar{T}_0(\bar{x}, \bar{t}) + \epsilon^2 \bar{T}_1(\bar{x}, \bar{r}, \bar{t}) + \dots ,$$

where $\bar{p}_a$ denotes the non-dimensional ambient pressure, defined in the obvious way by $p_a = (\mu_0 U L/h^2)\bar{p}_a$ and (from the continuity equation)

$$\bar{w}_0 = -\frac{\bar{r}\bar{u}_{0\bar{x}}}{2} + \frac{\bar{A}}{\bar{r}},$$

with the function $\bar{A}(\bar{x}, \bar{t})$ to be determined. Since from our *ansatz*, $\bar{T}$ (and thus the viscosity) is independent of $\bar{r}$ to leading order, it follows that, correct to $O(\epsilon^2)$, the $\bar{x}$-momentum equation is now

$$\mathrm{Re}[\bar{u}_{0\bar{t}} + \bar{u}_0\bar{u}_{0\bar{x}}] + \bar{P}_{\bar{x}} - \frac{\mathrm{Re}}{\mathrm{Fr}} - (2\bar{\mu}\bar{u}_{0\bar{x}})_{\bar{x}} + \bar{\mu}\bar{u}_{0\bar{x}\bar{x}} = \frac{1}{\bar{r}}(\bar{\mu}\bar{r}\bar{u}_{1\bar{r}})_{\bar{r}}, \tag{5}$$

and the $\bar{r}$-momentum yields $\bar{P}_{\bar{r}} = 0$, so that $\bar{P}$ is a function of $\bar{x}$ and $\bar{t}$ alone. The energy equation gives

$$\bar{T}_{0\bar{t}} + \bar{u}_0\bar{T}_{0\bar{x}} - \frac{1}{\mathrm{Re\,Pr}}(\bar{T}_{0\bar{x}})_{\bar{x}} - \Gamma(\bar{T}_a^4 - \bar{T}_0^4) = \frac{1}{\bar{r}\mathrm{Re\,Pr}}(\bar{r}\bar{T}_{1\bar{r}})_{\bar{r}}, \tag{6}$$

and to close the problem it is now necessary to specify kinematic conditions, normal and tangential stress conditions and temperature conditions on the free boundaries $\bar{h}_1$ and $\bar{h}_2$. The kinematic conditions are

$$\bar{w}_0 = \bar{h}_{1\bar{t}} + \bar{u}_0\bar{h}_{1\bar{x}} \quad \text{at} \quad \bar{r} = \bar{h}_1, \tag{7}$$

$$\bar{w}_0 = \bar{h}_{2\bar{t}} + \bar{u}_0\bar{h}_{2\bar{x}} \quad \text{at} \quad \bar{r} = \bar{h}_2. \tag{8}$$

As mentioned above, we wish to examine the possibility of controlling hole size by internal hole pressurisation. The normal-stress boundary conditions will thus include both the surface-tension coefficient γ and the fibre hole pressure p_H. If we define the non-dimensional fibre hole pressure by $p_H = (\mu_0 U L/h^2)\bar{p}_H$, it is clear that we must further write

$$\bar{p}_H = \bar{p}_a + \epsilon^2 \bar{p}_o, \tag{9}$$

where $\bar{p}_o$ is the non-dimensional hole overpressure. This scaling reflects the fact that, unless the fibre hole pressure is within $O(\epsilon^2)$ of the ambient pressure, the capillary will either collapse immediately or "explode". The Equation (9) therefore already gives a useful estimate of the size of hole-inflation pressure that is required to prevent collapse.

The normal-stress boundary conditions may now be applied. The stress tensor $\mathcal{T}$ is given by

$$\mathcal{T} = \frac{\mu_0 U}{L}\begin{pmatrix} -\bar{p}/\epsilon^2 + 2\bar{\mu}\bar{u}_{\bar{x}} & \bar{\mu}\bar{u}_{\bar{r}}/\epsilon + \epsilon\bar{\mu}\bar{w}_{\bar{x}} \\ \bar{\mu}\bar{u}_{\bar{r}}/\epsilon + \epsilon\bar{\mu}\bar{w}_{\bar{x}} & -\bar{p}/\epsilon^2 + 2\bar{\mu}\bar{w}_{\bar{r}} \end{pmatrix}.$$

If we now denote the unit outward-pointing normal to $\bar{r} = \bar{h}_i$ $(i = 1, 2)$ by $\hat{\boldsymbol{n}}_i$, then the normal-stress conditions are

$$-\hat{\boldsymbol{n}}_1^T \mathcal{T} \hat{\boldsymbol{n}}_1 + \frac{\bar{\gamma}\mu_0 U}{\bar{h}_1 L} = \frac{\bar{p}_H \mu_0 U}{L\epsilon^2} \quad \text{at } \bar{r} = \bar{h}_1,$$

$$-\hat{\boldsymbol{n}}_2^T \mathcal{T} \hat{\boldsymbol{n}}_2 - \frac{\bar{\gamma}\mu_0 U}{\bar{h}_2 L} = \frac{\bar{p}_a \mu_0 U}{L\epsilon^2} \quad \text{at } \bar{r} = \bar{h}_2.$$

Here a non-dimensional surface-tension coefficient has been defined by $\gamma = \mu_0 U \epsilon \bar{\gamma}$, thus immediately giving an estimate of the order of magnitude that the size of surface tension of the molten glass has to be to influence the final shape of the fibre.

We now assume that the tangential stress on both of the fibre boundaries is zero. Although this is evidently a good approximation, a "drag" term could be added at this stage if required. For $i = 1, 2$, we therefore have

$$\hat{\boldsymbol{t}}_i^T \bar{\mathcal{T}} \hat{\boldsymbol{n}}_i = 0,$$

where $\hat{\boldsymbol{t}}_i$ is the relevant unit tangent vector. To complete the specification of the boundary conditions, we assume that, because the thermal conductivity of air is much lower than than the thermal conductivity of glass, the fibre is essentially insulated on its inner surface. We also assume that it loses heat to the surrounding air in the furnace by Newton-type cooling at its outer surface (alternative thermal boundary conditions may be incorporated into the model at this stage if required). Thus (in dimensional variables)

$$T_r = 0 \quad \text{at} \quad r = h_1,$$

$$kT_r = N(T_a - T) \quad \text{at} \quad r = h_2,$$

where N is a heat-transfer coefficient that we assume for simplicity is constant and known from standard engineering correlations.

The normal and tangential stress conditions and thermal boundary conditions may now be expanded according to the *ansatz* for $\bar{u}$, $\bar{w}$ and $\bar{p}$. With

$$\hat{\boldsymbol{n}}_i^T = \frac{(-1)^{i+1}}{\sqrt{1+\epsilon^2\bar{h}_{i\bar{x}}^2}}(\epsilon\bar{h}_{i\bar{x}}, -1), \quad \hat{\boldsymbol{t}}_i^T = \frac{(-1)^{i+1}}{\sqrt{1+\epsilon^2\bar{h}_{i\bar{x}}^2}}(1, \epsilon\bar{h}_{i\bar{x}}),$$

we find that

$$-\frac{\bar{\gamma}}{\bar{h}_1} - \bar{P} + 2\bar{\mu}\bar{w}_{0\bar{r}} + \bar{p}_o = 0 \qquad \text{at} \quad \bar{r} = \bar{h}_1,$$

$$-\frac{\bar{\gamma}}{\bar{h}_2} - \bar{P} + 2\bar{\mu}\bar{w}_{0\bar{r}} = 0 \qquad \text{at} \quad \bar{r} = \bar{h}_2,$$

$$2\bar{h}_{1\bar{x}}(\bar{u}_{0\bar{x}} - \bar{w}_{0\bar{r}}) - \bar{w}_{0\bar{x}} = \bar{u}_{1\bar{r}} \qquad \text{at} \quad \bar{r} = \bar{h}_1,$$

$$2\bar{h}_{2\bar{x}}(\bar{u}_{0\bar{x}} - \bar{w}_{0\bar{r}}) - \bar{w}_{0\bar{x}} = \bar{u}_{1\bar{r}} \qquad \text{at} \quad \bar{r} = \bar{h}_2.$$

Expanded in non-dimensional variables, the thermal boundary conditions become

$$\bar{T}_{1\bar{r}} = 0 \quad \text{at} \quad \bar{r} = \bar{h}_1, \tag{10}$$

$$\bar{T}_{1\bar{r}} = \bar{N}(\bar{T}_a - \bar{T}_0) \quad \text{at} \quad \bar{r} = \bar{h}_2, \tag{11}$$

where $\bar{N} = LN/(\epsilon k)$ determines the relative importance of the Newton cooling, so that for small values of $\bar{N}$ the heat transfer is negligible, but for large $\bar{N}$ the condition is essentially $T = T_a$.

It is now possible to derive a closed system of leading-order equations for annular fibre drawing. We first multiply the x-momentum equation (5) by $\bar{r}$ and integrate from $\bar{r} = \bar{h}_1$ to $\bar{r} = \bar{h}_2$ to yield

$$\frac{(\bar{h}_2^2 - \bar{h}_1^2)}{2}\left[\mathrm{Re}(\bar{u}_{0\bar{t}} + \bar{u}_0\bar{u}_{0\bar{x}}) + \bar{P}_{\bar{x}} - \frac{\mathrm{Re}}{\mathrm{Fr}} - 2(\bar{\mu}\bar{u}_{0\bar{x}})_{\bar{x}} + \bar{\mu}\bar{u}_{0\bar{x}\bar{x}}\right] =$$

$$(\bar{\mu}\bar{h}_2\bar{u}_{1\bar{r}})\,|_{\bar{h}_2} - (\bar{\mu}\bar{h}_1\bar{u}_{1\bar{r}})\,|_{\bar{h}_1}\,. \tag{12}$$

Next, the energy equation (6) is multiplied through by $\bar{r}$ and integrated from $\bar{r} = \bar{h}_1$ to $\bar{r} = \bar{h}_2$ to yield

$$\left(\frac{\bar{h}_2^2 - \bar{h}_1^2}{2}\right)\left[\bar{T}_{0\bar{t}} + \bar{u}_0\bar{T}_{0\bar{x}} - \frac{1}{\mathrm{Re\,Pr}}(\bar{T}_{0\bar{x}})_{\bar{x}} - \Gamma(\bar{T}_a^4 - \bar{T}_0^4)\right] =$$

$$\frac{1}{\mathrm{Re\,Pr}}(\bar{h}_2\bar{T}_{1\bar{r}}\,|_{\bar{h}_2} - \bar{h}_1\bar{T}_{1\bar{r}}\,|_{\bar{h}_1}).$$

The kinematic conditions (7) and (8) now give

$$(\bar{h}_1^2)_{\bar{t}} + (\bar{h}_1^2\bar{u}_0)_{\bar{x}} = 2\bar{A}, \tag{13}$$

$$(\bar{h}_2^2)_{\bar{t}} + (\bar{h}_2^2\bar{u}_0)_{\bar{x}} = 2\bar{A}, \tag{14}$$

and the normal and tangential stress boundary conditions, when applied at $\bar{r} = \bar{h}_1$ and $\bar{r} = \bar{h}_2$, respectively, give

$$0 = -\frac{\bar{\gamma}}{\bar{h}_1} - \bar{P} + \bar{p}_o + \bar{\mu}\left(-\bar{u}_{0\bar{x}} - \frac{2\bar{A}}{\bar{h}_1^2}\right), \tag{15}$$

$$0 = \frac{\bar{\gamma}}{\bar{h}_2} - \bar{P} + \bar{\mu}\left(-\bar{u}_{0\bar{x}} - \frac{2\bar{A}}{\bar{h}_2^2}\right), \tag{16}$$

$$\bar{u}_{1\bar{r}}\,|_{\bar{r}=\bar{h}_1} = 2\bar{h}_{1\bar{x}}\left(\frac{3\bar{u}_{0\bar{x}}}{2} + \frac{\bar{A}}{\bar{h}_1^2}\right) - \frac{\bar{A}_{\bar{x}}}{\bar{h}_1} + \frac{\bar{h}_1\bar{u}_{0\bar{x}\bar{x}}}{2}, \tag{17}$$

$$\bar{u}_{1\bar{r}}\,|_{\bar{r}=\bar{h}_2} = 2\bar{h}_{2\bar{x}}\left(\frac{3\bar{u}_{0\bar{x}}}{2} + \frac{\bar{A}}{\bar{h}_2^2}\right) - \frac{\bar{A}_{\bar{x}}}{\bar{h}_2} + \frac{\bar{h}_2\bar{u}_{0\bar{x}\bar{x}}}{2}, \tag{18}$$

while the relevant temperature boundary conditions are (10) and (11). The equations (12)–(14) and (15)–(18) now constitute a system of seven equations in seven unknowns for the quantities $\bar{h}_1$, $\bar{h}_2$, $\bar{u}_0$, $\bar{P}$, $\bar{A}$, $\bar{u}_{1r}\,|_{\bar{r}=\bar{h}_1}$ and $\bar{u}_{1r}\,|_{\bar{r}=\bar{h}_2}$ These equations may now be greatly simplified. If we regard (15) and (16) as linear equations for $\bar{A}$ and $\bar{P}$, we find that

$$\bar{A} = \frac{\bar{p}_o\bar{h}_1^2\bar{h}_2^2 - \bar{\gamma}\bar{h}_1\bar{h}_2(\bar{h}_1+\bar{h}_2)}{2\bar{\mu}(\bar{h}_2^2-\bar{h}_1^2)}, \quad \bar{P} = \frac{\bar{\gamma}(\bar{h}_1+\bar{h}_2) - \bar{p}_o\bar{h}_1^2}{\bar{h}_2^2-\bar{h}_1^2} - \bar{\mu}\bar{u}_{0\bar{x}}.$$

When (17) and (18) are used in (12), a great deal of cancellation occurs, and the final (dimensional) equations that govern the drawing of a capillary become

$$\rho(h_2^2-h_1^2)[u_{0t}+u_0u_{0x}-g] = [3\mu(h_2^2-h_1^2)u_{0x} + \gamma(h_1+h_2)]_x, \tag{19}$$

$$(h_1^2)_t + (h_1^2u_0)_x = \frac{p_oh_1^2h_2^2 - \gamma h_1h_2(h_1+h_2)}{\mu(h_2^2-h_1^2)}, \tag{20}$$

$$(h_2^2)_t + (h_2^2u_0)_x = \frac{p_oh_1^2h_2^2 - \gamma h_1h_2(h_1+h_2)}{\mu(h_2^2-h_1^2)}, \tag{21}$$

$$\frac{(h_2^2-h_1^2)}{2}[\rho c_p(T_{0t}+u_0T_{0x}) - k(T_{0x})_x - \sigma\alpha(T_a^4-T_0^4)] = h_2N(T_a-T_0), \tag{22}$$

where $p_o = p_H - p_a$.

To fully close the problem (19)–(22), it is necessary to specify appropriate boundary and initial conditions. It is simplest to assume that h_1, h_2, u_0 and T_0 are all known as functions of x at time $t = 0$; for the majority of this study, however, we will be interested primarily in steady-state fibre manufacture. As far as boundary conditions are concerned, the preform geometry is invariably known, the feed speed is normally prescribed and the temperatures at the start and end of the draw are assumed to be given. At the furnace exit different boundary conditions may be appropriate for different regimes of fibre manufacture. For "caning" (the drawing of relatively large capillaries with outer diameters (ODs) of order mm) the capillaries are normally pulled by counter-rotating wheels that travel at a constant speed (for details see Figure 4 in Section 6.1). Some slip may occur between the drawn capillary and the wheels. Once drawn, these capillaries may later be stacked together to create a preform. Holey fibres are drawn from a preform of this type, and the finished product (which is very thin) is normally pulled onto a rotating drum. It may therefore not be quite clear whether the draw speed or the draw force is the appropriate condition to prescribe.

For definiteness, we shall assume that, unless otherwise stated, the boundary conditions for (19)–(22) are that the geometry of the capillary preform is known and that the feed and draw speeds are prescribed at $x = 0$ and $x = L$, respectively. Thus

$$h_1(0) = h_{10}, \quad h_2(0) = h_{20}, \quad u_0(0) = U_f, \quad u_0(L) = U_d,$$

$$T_0(0) = T_f, \quad T_0(L) = T_d. \tag{23}$$

It is worth pointing out that these should be regarded as lowest-order boundary conditions appropriate to our leading-order model, and that the full Navier-Stokes problem described by (1)–(4) would require additional boundary data to be fully specified.

3. Orders of magnitude of terms in the equations

In deriving (19)–(22) above we have deliberately exploited only the large aspect ratio of the fibre and have retained all other parameters in the analysis. In most drawing scenarios, however, some terms in the equations are small and may be neglected; this makes further simplifications possible. Many different drawing conditions are of practical interest: in caning the preform typically has an OD of between 4 and 20 mm. The inner diameters (IDs) of such capillary preforms usually range from 1·5 mm to 90% of the OD. Feed speeds tend to range between 0·5 and 5 mm/min and the final OD of the drawn capillary may range between 0·5 and 2·5 mm.

Holey fibres normally have a far more complex structure than the axisymmetric equations above can describe. We can, however, use the drawing conditions of a holey fibre to give some indication of the characteristic dimensions of interest. A single capillary within a multiple-hole holey-fibre preform is caned as above, and may subsequently be drawn down to an OD of 0·1–10 μm. A typical holey fibre may contain as many as 100 such capillaries occupying a total of between 10 and 100 μm of the final drawn fibre diameter. Typical draw speeds for holey fibres range between 10 and 50 m/min.

As far as material properties are concerned, both capillaries and holey fibres are routinely pulled from a very wide range of materials. Indeed, holey fibres have been fabricated from silica glasses of various grades, Gallium Lanthanum Sulphide glasses, and even polymers, at temperatures between a few hundred and 2300 °C. The drawing temperature inevitably reflects the viscosity at which viable drawing may take place. The majority of furnaces have a hot zone of length 1–5 cm. For many glasses accurate values for surface tension and its variation with temperature are not available. Values of about $\gamma = 0{\cdot}3$ N/m ([27], [28]) may be regarded as typical. As far as hole pressurisation is concerned, experimental studies (described later) indicate that values of p_o of up to a few p.s.i. (1 p.s.i. $\sim$ 6895 Pa) appear to be appropriate for some drawing regimes. Viscosities vary greatly with temperature and are frequently regarded as proprietary data: however, typical values are of order 10^4–10^5 kg/(m sec).

The relative importance of the terms appearing in the equations (19)–(22) may be estimated for the various drawing scenarios described above. If we rearrange (19) so that the viscosity term is multiplied by unity, then the relative importance of inertial, gravitational and surface tension effects are characterised respectively by the non-dimensional parameters

$$\frac{LU\rho}{\mu_0}, \quad \frac{gL^2\rho}{\mu_0 U}, \quad \frac{\gamma L}{Uh\mu_0}. \tag{24}$$

If we scale the left-hand sides of (20) and (21) so that the advective terms are unity, then the internal hole pressurisation and surface tension effects are similarly characterised by

$$\frac{Lp_o}{U\mu_0}, \quad \frac{\gamma L}{Uh\mu_0}. \tag{25}$$

Consideration of the regimes of practical interest outlined above yields a number of general conclusions: first, the non-dimensional parameters in (24) are never large compared to unity and hence viscosity effects are almost always important. Second, we find that inertial effects are invariably very small (though as we shall see in Section 5 below, they may influence the stability of the drawing process). Gravitational effects are more important in caning than in the drawing of holey fibres, and in many regimes surface tension and viscous effects compete. As far as the parameters in (25) are concerned, we find that surface-tension effects are normally non-negligible. Finally, the non-dimensional parameter $Lp_o/U\mu_0$ in (25) needs to be of order unity for internal pressurisation effects to be significant.

Analysis of the temperature equation (22) may be carried out in the same way as above, but is greatly complicated by uncertainties in the coefficients k and N. If both the diffusion and the surface heat transfer are essentially determined by radiative-heat-transfer effects, then diffusion, bulk heating and surface heat transfer will all assume the same importance. It is also evident that the advective terms in (22) may be important when temperatures are low or the draw speed is large.

4. Asymptotic limits of the model

The general equations (19)–(22) may now be examined in a number of asymptotic limits. These special cases can give valuable information relevant to the manufacture of both capillaries and fibres.

First, we note that solid fibres have been analysed using extensional flow arguments similar to those described above on a number of occasions. These models therefore provide a partial check on (19)–(22). In particular, if we consider isothermal solid-fibre drawing and set $h_1 = 0$, and $h_2 = H$, then we find that (21) and (19) become

$$(H^2)_t + (H^2u_0)_x = 0, \quad \rho H^2(u_{0t} + u_0u_{0x} - g) = [3\mu H^2u_{0x} + \gamma H]_x,$$

which is in exact agreement with (for example) [16].

4.1. Shape-preserving steady similarity solution

A number of simple steady solutions are available to (19)–(22) when internal hole pressure, surface tension, inertial and gravity effects are ignored. Under these assumptions, the equations become

$$(3\mu(h_2^2 - h_1^2)u_{0x})_x = 0,$$

$$(h_1^2u_0)_x = (h_2^2u_0)_x = 0,$$

$$\frac{(h_2^2 - h_1^2)}{2}[k(T_{0x})_x - \sigma\alpha(T_a^4 - T_0^4)] = h_2N(T_a - T_0).$$

Assuming that the boundary conditions (23) apply, we quickly find that

$$h_1^2u_0 = h_{10}^2U_f, \quad h_2^2u_0 = h_{20}^2U_f, \tag{26}$$

and

$$\log\left(\frac{u_0}{U_f}\right) = \beta\left(\int_0^x \frac{d\xi}{\mu(T(\xi))}\right) / \left(\int_0^L \frac{d\xi}{\mu(T(\xi))}\right), \tag{27}$$

where

$$\beta = \log(U_d/U_f).$$

Given a known functional form for the viscosity as a function of temperature, we may now complete the solution by solving the temperature equation. The simplest case occurs when μ is independent of temperature (or when drawing is isothermal so that $T_0 = T_a$). In this case, we have

$$u_0 = U_f \mathrm{e}^{\beta x/L}, \quad h_1 = h_{10}\mathrm{e}^{-\beta x/2L}, \quad h_2 = h_{20}\mathrm{e}^{-\beta x/2L}.$$

When the viscosity depends upon temperature and the furnace temperature profile $T_a(x)$ may be directly measured, (27) may be used under the assumption that $T(x) \approx T_a(x)$ to quantify the details of the drawing process as a function of the furnace profile.

Whatever the dependence of μ on temperature, we note from (26) that the absence of surface tension and internal hole pressurisation means that the initial fibre geometry is always preserved throughout the pull, and there is no question of hole closure or fibre "explosion". This is essentially a consequence of the fact that, at this level of approximation, no forces act in the plane of the fibre cross-section.

4.2. The effects of fibre inertia and gravity

Some analytical progress may also be made in quantifying the effects of inertia. If we consider steady flow and ignore temperature variations, gravity, hole pressurisation and surface tension then (19)–(21) become

$$\rho(h_2^2 - h_1^2)u_0u_{0x} = [3\mu(h_2^2 - h_1^2)u_{0x}]_x, \quad (h_1^2u_0)_x = 0, \quad (h_2^2u_0)_x = 0.$$

These equations may be solved using standard methods, and when the boundary conditions (23) are applied, we find that

$$u_0 = \frac{3U_f\mu\kappa\mathrm{e}^{\kappa x}}{3\mu\kappa + \rho U_f(1-\mathrm{e}^{\kappa x})},$$

$$h_1 = h_{10}\sqrt{\frac{3\mu\kappa + \rho U_f(1-\mathrm{e}^{\kappa x})}{3\mu\kappa\mathrm{e}^{\kappa x}}},$$

$$h_2 = h_{20}\sqrt{\frac{3\mu\kappa + \rho U_f(1-\mathrm{e}^{\kappa x})}{3\mu\kappa\mathrm{e}^{\kappa x}}},$$

where the constant κ satisfies the transcendental equation

$$\mathrm{e}^{\beta} = \frac{U_d}{U_f} = \frac{\mathrm{e}^{\kappa L}}{\frac{\rho U_f}{3\mu\kappa}(1-\mathrm{e}^{\kappa L})+1}. \tag{28}$$

We note first that the ratio h_1/h_2 remains constant. Inertia cannot therefore affect the fibre geometry ratio. Some elementary analysis may be used to show that for physically relevant cases where $U_d \geq U_f$, $\tilde{\rho} \geq 0$, (28) always possesses a solution (where we have written $\tilde{\rho} = \rho U_f L/3\mu$). A special case arises when precisely $\mathrm{e}^{\beta} = 1/(1-\tilde{\rho})$, in which case $\kappa = 0$ is the only solution and the fibre velocity has algebraic behaviour. Otherwise, it is easy to show

that if $\tilde{\rho} \geq 1$ we have $\kappa < 0$. Further, if $0 < \tilde{\rho} < 1$ then we have $\kappa > 0$ for $e^{\beta} > 1/(1-\tilde{\rho})$, and $\kappa < 0$ for $e^{\beta} < 1/(1-\tilde{\rho})$. In practice, we expect that the ratio $\tilde{\rho}$ is always likely to be small. In the theoretical (but practically unlikely) case of $\tilde{\rho}$ large, it may also be shown that there is a boundary layer near to $x = L$. This implies that a very dense fibre travels at its feed speed for most of the draw until just before the end of the furnace.

It is also worth mentioning that some progress may be made when the fibre inertia is neglected, but gravity is re-introduced into the equations. We find that

$$u_0 = \frac{C_1^2 e^{2C_1(x+C_2)} - 2C_1\phi e^{C_1(x+C_2)} + \phi^2}{2C_1^3 e^{C_1(x+C_2)}},$$

$$h_1 = h_{10}\sqrt{\frac{U_f}{u_0}}, \quad h_2 = h_{20}\sqrt{\frac{U_f}{u_0}},$$

where $\phi = \rho g/3\mu$ and C_1 and C_2 are constants that satisfy simultaneous transcendental equations. The effect of including gravity is thus similar to that of including inertia: the fibre speed and the internal and external diameters are modified, but the initial hole geometry is still preserved throughout the draw.

4.3. The effects of surface tension

Thus far all asymptotic limits that we have considered have preserved the initial preform geometry. In practice, however, when capillaries or holey fibres are drawn, surface tension can lead to significant geometry changes and even hole collapse.

Some analytical progress may be made in the steady isothermal case where internal hole pressurisation, gravity and inertia are ignored, but the effects of surface tension are retained. Equation (19) may be integrated to give

$$3\mu(h_2^2 - h_1^2)u_{0x} = F_d - \gamma(h_1 + h_2), \tag{29}$$

where F_d is a constant that amounts precisely to the total force applied to the fibre. Subtracting (20) from (21) we have

$$(h_2^2 - h_1^2)u_0 = C, \tag{30}$$

where the constant C measures the mass flux of the draw. We now regard (29) and (30) as formulae for u_0 and u_{0x}, expand out equations (20) and (21), substitute for u_0 and u_{0x} and then divide to obtain

$$\frac{dh_2}{dh_1} = \frac{\gamma(h_1 + h_2)(h_2 - 3h_1) - F_d h_2}{\gamma(h_1 + h_2)(h_1 - 3h_2) - F_d h_1}. \tag{31}$$

Elementary methods may now be used to integrate (31), giving

$$\frac{(h_2 - h_1)^{1/3}}{(h_2 + h_1)^{1/3}}[2\gamma(h_1 + h_2) + F_d] = D, \tag{32}$$

where D is a constant that may be found simply by evaluating the left-hand side of (32) at $x = 0$. In reality, (32) is not as helpful as it might seem. In principle, it is possible to solve for h_2 in terms of h_1 so that we may determine u_0 as a function of h_2 using (30), and the full solution may then be found using (29), but the equation connecting h_1 and h_2 is a quartic which

complicates matters considerably. Furthermore, the constant F_d is not in general known, since, as discussed above, the most common prescription of the fibre-drawing problem specifies the feed and draw speeds but gives no information concerning the fibre acceleration at either end. In spite of this, one may argue (as at the end of Section 2) that, though the draw speed is often prescribed, there may be slippage, thereby dictating the force applied at the fibre winder. In this case, the constant F_d may be regarded as known and (32) may be used immediately to show that hole closure ($h_1 = 0$) takes place when the outer diameter of the fibre is given by

$$h_2 = h_{20}\left((1-a)^{1/3}(1+a)^{2/3} - \frac{F_d}{2\gamma h_{20}}\left(1 - \left(\frac{1-a}{1+a}\right)^{1/3}\right)\right), \tag{33}$$

where the preform geometry ratio a is defined by $a = h_{10}/h_{20}$. This equation provides some insight into the minimum outer diameter capillary that may be drawn from a given preform before inner hole closure occurs. Given the physical condition $0 < a < 1$ we note that capillaries with smaller ODs where the inner hole remains intact may be drawn by using larger draw forces and/or smaller surface tensions. If, as is normally the case, the OD of the drawn fibre is required to be significantly smaller than the preform, then (33) asserts that the quantity multiplying h_{20} on the right-hand side of (33) must be small, and thus

$$F_d \approx \frac{2\gamma h_{20}(1+a)(1-a)^{1/3}}{(1+a)^{1/3} - (1-a)^{1/3}}.$$

We may interpret this result for both thick- and thin-walled tubes: for thick-walled capillaries ($a \ll 1$) the minimum outer diameter that may be drawn before collapse occurs is

$$h_{20}\left(1 - \frac{F_d a}{3\gamma h_{20}}\right).$$

We therefore require $F_d \approx 3\gamma h_{20}^2/h_{10}$, which suggests that closure of the inner hole is very sensitive to the quantity F_d.

For thin-walled capillaries ($a \sim 1$) the minimum OD that can be drawn is

$$h_{20}\left((4(1-a))^{1/3} - \frac{F_d}{2\gamma h_{20}}\right),$$

which, for reasonable drawing conditions, implies that $F_d \approx 2\gamma h_{20}(4(1-a))^{1/3}$. Once again, this shows that collapse is very sensitive to draw force.

4.4. Small-surface-tension limit

In the previous subsection we were able to draw some conclusions for arbitrarily sized capillaries subject to arbitrary surface-tension forces. Still more analytical progress may be made when the non-dimensional ratio $\delta = \gamma L/(\mu h U)$ is much less than unity, so that the effects of surface tension are present, but "small". As before, we consider the isothermal version of the governing equations when inertia and gravity are neglected, and there is no internal hole pressurisation.

In Section 6, we will present comparisons with experiments that were performed under precisely these conditions; the study of this viscosity-dominated limiting case of the equations is thus particularly relevant. Under such conditions, we may therefore conveniently regard (19)–(21) as a regular perturbation problem in δ. Solving the equations now becomes a simple matter, and we find that

$$u_0 = U_f e^{\beta x/L} + \frac{2\gamma L e^{\beta x/L}}{3\mu\beta(h_{20}-h_{10})} \times \left[e^{-\beta x/2L} - 1 + \left(\frac{x}{L}\right)(1 - e^{-\beta/2})\right], \tag{34}$$

$$h_1 = h_{10} e^{-\beta x/2L} + \frac{\gamma L e^{-\beta x/L}}{3\mu\beta U_f(h_{20}-h_{10})} \times \left[(3h_{20}-h_{10})(1 - e^{\beta x/2L}) + \left(\frac{h_{10}x}{L}\right) e^{\beta x/2L}(e^{-\beta/2}-1)\right], \tag{35}$$

$$h_2 = h_{20} e^{-\beta x/2L} + \frac{\gamma L e^{-\beta x/L}}{3\mu\beta U_f(h_{20}-h_{10})} \times \left[(3h_{10}-h_{20})(1 - e^{\beta x/2L}) + \left(\frac{h_{10}x}{L}\right) e^{\beta x/2L}(e^{-\beta/2}-1)\right], \tag{36}$$

where once again $\beta = \log(U_d/U_f)$.

Equations (34)–(36) allow the prediction of the degree of collapse in the final structure, which depends only upon the ratio of the surface tension to the viscosity. We also note that the temperature dependence of this problem manifests itself only via this ratio of the surface tension to the viscosity. We may employ (35) to re-examine hole collapse. By setting $h_1 = 0$ in (35) we find that collapse occurs exactly at $x = L$ when

$$h_{10} = \frac{\gamma L h_{20}}{\mu\beta U_f(h_{20}-h_{10})}(1 - e^{-\beta/2}).$$

A good approximation to this condition may be gained by noting that $e^{-\beta/2} = \sqrt{U_f/U_d}$ which, for the purposes of the current study, may be regarded as negligible compared to one. Hole collapse at or before $x = L$ thus occurs when

$$\mu U_f \log(U_d/U_f) \leq \frac{\gamma L h_{20}}{h_{10}(h_{20}-h_{10})}. \tag{37}$$

For a given preform, material and furnace, we may regard the right-hand side of (37) as known. As far as the control parameters U_d and U_f are concerned, therefore, we conclude that, in this regime, hole collapse is more sensitive to the feed speed than the draw speed. Also, we note that the effect of changing the furnace temperature enters (37) via the parameter μ and so, not surprisingly, the phenomenon of hole closure is sensitive to temperature.

4.5. The role of internal hole pressure

One obvious way of controlling the degree of hole closure and preventing collapse is to introduce a pressure difference between the air inside and outside the capillary. To begin to quantify the effects of hole pressurisation, we first study (19)–(22) assuming a steady isothermal draw and that the effects of inertia, gravity and surface tension are ignored. The problem that must then be solved reduces to

$$[(H_2 - H_1)u_{0x}]_x = 0, \quad (H_1 u_0)_x = (H_2 u_0)_x = \frac{p_o H_1 H_2}{\mu(H_2 - H_1)},$$

where we have written $H_1 = h_1^2$ and $H_2 = h_2^2$. When the two mass-conservation equations are subtracted, we find that $(H_2 - H_1)u_0 = (H_{20} - H_{10})U_f$ (where $H_{10} = H_1(0)$, $H_{20} = H_2(0)$). We may now use elementary methods to solve the governing equations. These yield

$$u_0 = U_f \mathrm{e}^{\beta x/L},$$

$$H_1 = \frac{H_{10}(H_{20} - H_{10})\mathrm{e}^{-\beta x/L}}{H_{20}\exp\left[\frac{p_o L}{U_f \mu\beta}(\mathrm{e}^{-\beta x/L} - 1)\right] - H_{10}},$$

$$H_2 = \frac{H_{20}(H_{20} - H_{10})\mathrm{e}^{-\beta x/L}}{-H_{10}\exp\left[\frac{p_o L}{U_f \mu\beta}(-\mathrm{e}^{-\beta x/L} + 1)\right] + H_{20}},$$

so that

$$\frac{H_1}{H_2} = a^2 \exp\left[\frac{p_o L}{U_f \mu\beta}(1 - \mathrm{e}^{-\beta x/L})\right].$$

Though the fibre speed is therefore not influenced by internal hole pressurisation, the fibre no longer preserves its initial inner/outer geometry ratio. At the end of the draw when $x = L$ we have

$$\frac{H_1}{H_2} = a^2\, \mathrm{e}^{Q},$$

where

$$Q = \frac{p_o L(U_d - U_f)}{\mu U_f U_d \beta}.$$

Since H_1/H_2 increases without limit as $p_o \to \infty$, we may anticipate that under some circumstances the fibre may "explode". The expressions for H_1 and H_2 confirm that both become unbounded when

$$x = -\frac{L}{\beta}\log\left[1 + \frac{2U_f \mu\beta}{p_o L}\log a\right].$$

Since the draw takes place over the region $0 \le x \le L$, there is therefore no hope of achieving a controlled manufacturing process if

$$p_o \ge \frac{2U_f \mu\beta \log a}{L(\mathrm{e}^{-\beta} - 1)}. \tag{38}$$

Although, of course, surface-tension effects have been ignored in deriving (38), this expression nevertheless provides a good practical upper bound for the amount of hole pressurisation that may be used for given draw. Evidently larger hot zone lengths L, smaller viscosities μ and smaller feed speeds U_f all decrease the critical value of p_o and therefore increase experimental sensitivity. This suggests that, though internal hole pressurisation might be employed to prevent hole collapse, it may lead to drawing processes that are harder to control.

4.6. Closure of a small hole

In practice we would like to understand the interplay between surface tension and hole pressurisation. When the effects of hole pressurisation and surface tension are both included, (31) becomes

$$\frac{\mathrm{d}h_2}{\mathrm{d}h_1} = \frac{\gamma(h_1+h_2)(h_2-3h_1) - F_d h_2 + 3p_o h_1^2 h_2}{\gamma(h_1+h_2)(h_1-3h_2) - F_d h_1 + 3p_o h_1 h_2^2}. \tag{39}$$

Unfortunately, this equation cannot be solved in closed form to yield h_2 in terms of h_1. Although it is possible to carry out a phase-plane analysis of (39) (there are 7 singular points), this does not appear to lead to any very valuable conclusions.

A less general but more illuminating approach is to consider the fate of a "small" hole during a steady isothermal draw. Since there are many practical circumstances in which we wish to produce fibres with small holes, it is particularly important to understand this regime and to be able to explore parameters that may be exploited to avoid hole closure. As the internal capillary hole begins to close off, we may expect that, apart from the hole pressurisation, the important governing forces will be the viscosity and the surface tension. We therefore ignore inertial and gravitational effects in the Equations (19)–(21) and scale by setting $h_1 = \delta h \bar{h}_1$ and $h_2 = h\bar{h}$ where δ is small. The surface tension must also be scaled using δ, since a small hole would instantly close for a surface tension of order $\mu_0 U \epsilon$. Under these assumptions, the (redimensionalised) equations become, to leading order,

$$(3\mu h_2^2 u_{0x})_x = 0, \tag{40}$$

$$(h_2^2 u_0)_x = 0, \tag{41}$$

$$(h_1^2 u_0)_x = \frac{p_o h_1^2}{\mu} - \frac{\gamma h_1}{\mu}, \tag{42}$$

Both (40) and (41) may be solved as before to yield

$$h_2 = h_{20}\exp(-\beta x/L), \quad u_0 = U_f \exp(\beta x/L),$$

and (42) therefore becomes simply

$$(h_1^2 \mathrm{e}^{\beta x/L})_x = \frac{p_o}{\mu U_f} h_1^2 - \frac{\gamma}{\mu U_f} h_1, \tag{43}$$

subject to the boundary condition $h_1(0) = h_{10}$ where $h_{10} = O(\delta h)$. Equation (43) may be solved in closed form; we find that either $h_1 = 0$ or

$$h_1 = \exp\left(-\frac{\beta x}{2L} - P\mathrm{e}^{-\frac{\beta x}{L}}\right)\left[h_{10}\mathrm{e}^{P} - \int_0^x G\exp\left(-\frac{\beta u}{2L} + P\mathrm{e}^{-\frac{\beta u}{L}}\right)\mathrm{d}u\right].$$

where the non-dimensional parameters P and G are defined by $P = (p_o L)/(2\beta\mu U_f)$ and $G = \gamma/(2\mu U_f)$. Some observations about this solution are now in order. First, we note that the only constant solution to (43) is $h_1 = 0$. Moreover, by observing that at stationary points when $h_{1x} = 0$ we have $h_{1xx} = -\beta^2 h_1/2L^2$, it follows that every solution to (43) can have at most one maximum (which must occur when h_1 is positive), and at most one minimum (which must occur when h_1 is negative). The case of $h_1 < 0$ is, of course, unphysical. It is worth observing that the solutions to (43) exhibit some interesting behaviour from what is, essentially only a first-order linear ordinary differential equation.

It is now simplest to regard h_{10}, γ, μ, U_f, L and β as known and classify solutions according to the size of the internal hole pressure, and thus P. As in previous sections, one key question concerns whether or not h_1 reaches 0 before the end of the draw. The condition that the internal hole closes at or before $x = L$ is that p_o is less than or equal to the value defined by

$$G\int_0^L \exp\left(-\frac{\beta u}{2L} + P\mathrm{e}^{-\beta u/L}\right)\,\mathrm{d}u = h_{10}\mathrm{e}^P. \tag{44}$$

and this may be regarded as a condition for "fibre collapse".

As far as "fibre explosion" is concerned, it is an obvious consequence of our analysis for small holes that (43) cannot be expected to lead to solutions that become unbounded; in any case, the model would be invalid if this were to occur. Fibre explosion can still be investigated, however. The condition that $h_1'(0) > 0$ amounts to

$$p_o > \frac{\gamma}{h_{10}} + \frac{\beta\mu U_f}{L}. \tag{45}$$

Internal hole pressures greater than this may therefore be regarded as leading to "hole expansion" where, for at least some part of the draw, the internal hole is increased in size.

It is, of course, not obvious how much expansion could be tolerated before a fibre would actually explode but the expression (45) gives a reasonable conservative criterion for such pressurisation. One might, for example, guess that in practice fibre explosion would take place whenever h_1 becomes so large that $h_1 > h_{20}$. The real value of (43), however, is the clue that it gives to the sensitivity of the pressurised drawing of a fibre. If we simplify (43) to read $h_1 = 0$ or

$$h_{1x} = h_1\left(\frac{P\beta}{L}\mathrm{e}^{-\beta x/L} - \frac{\beta}{2L}\right) - G\mathrm{e}^{-\beta x/L},$$

then we see that the pressurisation term never contributes significantly to the solution unless $P \geq 1/2$. Furthermore, if $G \gg \beta h_{10}/2L$, the solution is particularly sensitive to the level of hole pressurisation. The "sensitivity parameter"

$$S = \frac{2LG}{\beta h_{10}} = \frac{L\gamma}{\mu h_{10} U_f \log(U_d/U_f)}$$

is thus the key parameter as far as the practicability of pressurised fibre drawing is concerned. When $S \ll 1$ internal hole pressurisation might be a valid experimental control mechanism: if $S \gg 1$ then hole pressurisation is simply not worth considering.

4.7. Solutions to the full problem

When inertia, gravity, surface tension and hole pressurisation are included in (19)–(22) the equations must be solved numerically. Though the numerical solution of the unsteady versions of the equations is a fairly routine matter, our main interest is to analyse the steady-state manufacturing process for capillaries. With time derivatives set equal to zero, (19)–(22) constitute an ordinary-differential-equation two-point boundary-value problem which may be solved using standard library routines. In particular, we used the NAG routine D02HAF which employs an efficient Runge-Kutta-Merson method (see, for example [29, Chapter 5]. Provided that a good estimate can be found for $u_{0x}(0)$, this method is reliable and accurate. In this way solutions may be computed for arbitrary values of the experimental parameters.

5. Stability of the drawing process

As far as the industrial process of drawing annular fibres is concerned, the stability of the process is obviously a key issue. For instance, is the process sensitive to small changes in

the experimental equipment or conditions? More importantly, is the process stable enough to suggest that long lengths of fibre or capillary with uniform structure can be produced? Before considering the stability of capillary drawing, it is helpful to consider first the case of solid fibres.

5.1. STABILITY FOR SOLID FIBRES

The simplest isothermal stability analysis for a solid fibre is easy to carry out and has been addressed many times before (see, for example [30], [8], or [28]). We briefly repeat the main points of the analysis for convenience. Neglecting inertia, gravity and surface tension in (19) and (21), setting $h_1 = 0$ and writing $A(x,t) = \pi h_2^2(x,t)$, we find that the time-dependent governing equations are

$$A_t + (Au_0)_x = 0, \qquad (Au_{0x})_x = 0. \tag{46}$$

To examine stability we now set

$$u_0 = U_0(x)[1 + u(x)\mathrm{e}^{\sigma t}],$$

and

$$A = A_0(x)[1 + a(x)\mathrm{e}^{\sigma t}],$$

where $U_0 = U_f \exp(\beta x/L)$, $A_0 = A_f \exp(-\beta x/L)$ are the steady-state solutions, A_f is the initial fibre cross-sectional area and a, u and σ are complex. Assuming in the normal way that u and a are "small", we find that at first order

$$\sigma a + U_f \mathrm{e}^{\beta x/L}(a' + u') = 0, \tag{47}$$

and

$$u'' + \left(\frac{\beta}{L}\right)(u' + a') = 0, \tag{48}$$

the boundary conditions being $a(0) = u(0) = u(L) = 0$. On elimination of u, we find that a satisfies

$$a'' + \frac{\sigma \mathrm{e}^{-\beta x/L}}{U_f} a' = 0. \tag{49}$$

The solution of this equation that satisfies $a(0) = 0$ is

$$a = B\left[-\mathrm{Ei}\left(1, -\frac{\sigma L}{\beta U_f}\right) + \mathrm{Ei}\left(1, -\frac{\sigma L \mathrm{e}^{-\beta x/L}}{\beta U_f}\right)\right], \tag{50}$$

where B is an arbitrary constant and as usual the exponential integral function $\mathrm{Ei}(n,x)$ is defined by

$$\mathrm{Ei}(n,x) = \int_1^\infty \frac{\mathrm{e}^{-xt}}{t^n}\mathrm{d}t.$$

By integrating (48) from 0 to L and evaluating (47) at both 0 and L, we find that a second boundary condition for (49) is given by

$$a'(L) - a'(0) + a(L)\left[\frac{\sigma}{U_f}\mathrm{e}^{-\beta} - \frac{\beta}{L}\right] = 0,$$

and applying this to (50) (having set $\xi = \sigma L/(\beta U_f)$) we have the condition

$$\mathrm{e}^{\xi \mathrm{e}^{-\beta}} - \mathrm{e}^{\xi} + [1 - \xi \mathrm{e}^{-\beta}][\mathrm{Ei}(1, -\xi) - \mathrm{Ei}(1, -\xi \mathrm{e}^{-\beta})] = 0. \tag{51}$$

In any given fibre-drawing experiment β, U_f and L are given. The stability problem therefore consists of establishing under what circumstances the complex equation (51) possesses solutions for ξ with positive real parts: these are the unstable cases. Some fairly routine numerical calculations show that, as β increases from zero, (51) has a purely imaginary root when $\beta \sim 3{\cdot}00651$ and thus the celebrated "draw resonance" (see, for example [21]) for solid fibres occurs when $U_d/U_f \sim 20{\cdot}21$. In theory, this places a very severe restriction on fibre drawing as draw ratios are normally a great deal higher than 20. Of course, this simple analysis has ignored the effects of gravity, inertia, temperature and surface tension. Numerical studies for a solid fibre (see, for example [31], [14], [28] and [9]) show that essentially (as might be expected) inertia and gravity stabilise the process, but surface tension is a destabilising factor. Normally these effects are rather small though, and this begs the question as to how (as they routinely are) fibres can be manufactured with highly supercritical draw ratios. The answer lies in the fact that, as already alluded to in Section 2, though ostensibly the draw speed is prescribed, in reality some control of the force occurs owing to slippage at the exit winder. Carrying out the same sort of analysis as above but with boundary conditions

$$u_0(0) = U_f, \qquad A(0) = A_f, \qquad A(L)u_{0x}(L) = F_d,$$

gives $U_0 = U_f \exp(\chi x)$, $A_0 = A_f \exp(-\chi x)$ where $\chi = F_d/A_f U_f$. The stability equation (49) becomes

$$a'' + \frac{\sigma \mathrm{e}^{-\chi x}}{U_f} a' = 0,$$

and the solution with $a(0) = 0$ is thus

$$a = B\left[-\mathrm{Ei}\left(1, -\frac{\sigma}{\chi U_f}\right) + \mathrm{Ei}\left(1, -\frac{\sigma \mathrm{e}^{-\chi x}}{\chi U_f}\right)\right].$$

However, since in this case the boundary conditions are $u(0) = 0$, $a(0) = 0$ and $u'(L) + \chi(u(L) + a(L)) = 0$, we find that $a'(0) = 0$, the problem is an initial-value one and therefore no unstable modes exist.

5.2. Stability for capillary drawing

What of stability for capillary drawing? When inertia, gravity, surface tension and internal hole pressurisation are ignored, simply adding (20) to (21) shows that the equations that determine the stability of a capillary are essentially identical to (46), save for the fact that, once the stability or otherwise of the draw has been established for a fibre of given cross-sectional area, an extra equation is required to determine the details of the evolution of disturbances to the inner and outer fibre radii. Most of the conclusions of Section 5.1 are thus identical for capillaries. When surface tension and internal hole pressurisation are added, however, matters are significantly complicated. Though we have observed that surface tension destabilises a solid fibre, it is not at all clear if this conclusion will still hold for a capillary. The role of

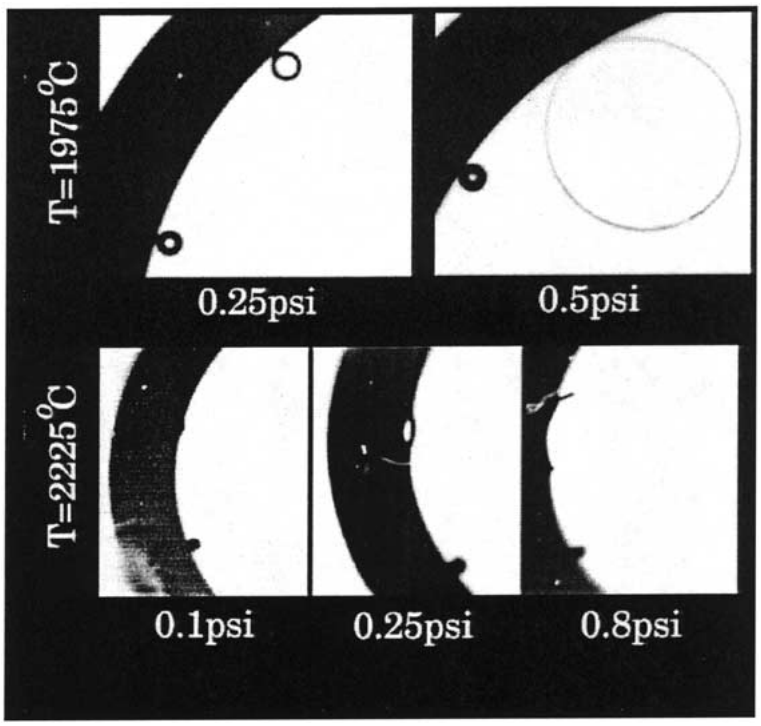

Figure 3. Results from tests of active silica capillary pressurisation. Two small capillaries attached to the wall of a larger tube are drawn using a standard fibre drawing tower for a range of temperatures and overpressures. In each case the lower of the two small capillaries is a control with no overpressure.

internal pressure in stability calculations is also opaque, though it seems intuitively obvious that inertia and gravity will still act as stabilising mechanisms. The numerical calculations that are required to confirm these conjectures are of a routine but somewhat involved nature; we therefore postpone them to a further study.

6. Comparisons with experiment

In order to test the model, some simple capillary drawing experiments were performed. First, some preliminary draws were performed using standard silica glass, and various amounts of hole pressurisation. Our aim was to see whether the asymptotic results contained in Section 4 were qualitatively accurate.

Figure 3 shows the results of two experiments. The preform consisted of a large silica capillary (OD=20mm, ID=16mm) to whose inside wall two small silica capillaries were attached. The only function of the larger outer capillary is to support the small test capillaries, so that we can preserve the remnants of any capillaries that may have exploded. These would otherwise vanish without trace, leaving no evidence of their presence.

The initial attached capillary inner and outer radii were $h_{10} = 0{\cdot}64$ mm and $h_{20} = 0{\cdot}8$mm respectively. The preform was drawn using a standard fibre drawing tower (described more fully in Section 6.1). Experiments were carried out at temperatures of 1975 °C and 2225 °C. For both experiments the feed and draw speeds were $U_f = 2{\cdot}6\times10^{-5}$ m/sec and $U_d = \frac{1}{6}$ m/sec respectively and the hot zone length was $L = 0{\cdot}03$m. In each case pictured in Figure 3, the

upper small capillary was maintained at a specified overpressure, and the lower small capillary was unpressurised and therefore acted as a control.

At a temperature of 1975 °C, the control capillary remains open, but has experienced a significant amount of collapse during the drawing process. For the upper capillary in Figure 3 with an overpressure of 0·25p.s.i at this temperature, this collapse has been avoided. At the somewhat larger overpressure of 0·5p.s.i. the upper capillary has inflated dramatically, though it has not actually "exploded".

When the temperature is raised to 2225 °C, the control capillary closes completely under the action of surface tension. The smallest overpressure of 0·1p.s.i. is evidently insufficient to arrest the collapse of the upper capillary. When the overpressure is increased to 0·25p.s.i., the hole does not collapse though it is deformed significantly by the action of surface tension. At the greatest overpressure of 0·8p.s.i. the pressurised capillary has "exploded" and only its ragged edges (the remnants of the original capillary) remain.

Consider now the results from Subsections 4.5 and 4.6: in 4.5 we saw that the critical pressure for fibre explosion was given by

$$p_o = \frac{2U_f \mu\beta \log a}{L(\mathrm{e}^{-\beta} - 1)}. \tag{52}$$

Assuming that (in S.I. units) the viscosity of the glass is given by the Fulcher law (see, for example [27])

$$\mu = 0{\cdot}1 \times 10^{-6{\cdot}24 + 26900/(T+273)}$$

where the temperature T is measured in degrees centigrade, and that the surface tension of the glass is $\gamma = 0{\cdot}3$ N/m, (52) gives critical explosion pressures of $p_o = 180{\cdot}5$Pa ($T = 1975$ °C), $p_o = 11{\cdot}5$Pa ($T = 2225$ °C). Evidently these values are far too low, since from Figure 3 it appears that fibre expansion (but no explosion) takes place at the lower temperature, whereas fibre explosion takes place for some value of p_o between 0·25 and 0·8 p.s.i. (*i.e.* 1724–5516Pa). This disagreement is to be expected since the asymptotics used to arrive at (52) ignored the contracting effects of surface tension completely and should therefore be expected to produce an underestimate of the critical pressure.

Let us now use the "small hole" theory of Section 4.6 for comparison purposes. We recall that the condition for collapse at $x = L$ is given by (44). When we solve (44) numerically to determine P (and thus p_o) using the experimental parameters described above, we find that $p_o = 167$Pa $\sim 0{\cdot}02$p.s.i. when $T = 1975$ °C, whilst $p_o = 498$Pa $\sim 0{\cdot}07$p.s.i. when $T = 2225$ °C. These results are much more encouraging, for we see from Figure 3 that collapse almost takes place at the lower temperature in the control capillary, while collapse takes place for $p_o = 0.1$p.s.i. ~ 690Pa at the higher temperature.

As noted in Section 4.6 it is harder to propose an "explosion" criterion. It is interesting, however, to calculate the quantity

$$p_o = \frac{\gamma}{h_{10}} + \frac{\beta\mu U_f}{L},$$

which is the condition that $h_{1x}(0) > 0$. This is given by $p_o = 873$Pa for a temperature of 1975 °C and 494Pa for a temperature of 2225 °C. Recalling the discussion of Section 4.6, we expect fibre expansion and subsequent explosion to take place for some hole pressure above these values of p_o, and this seems to agree qualitatively with the experimental results. Finally, it is interesting to calculate the "sensitivity parameter" S that was identified in Section 4.6. We

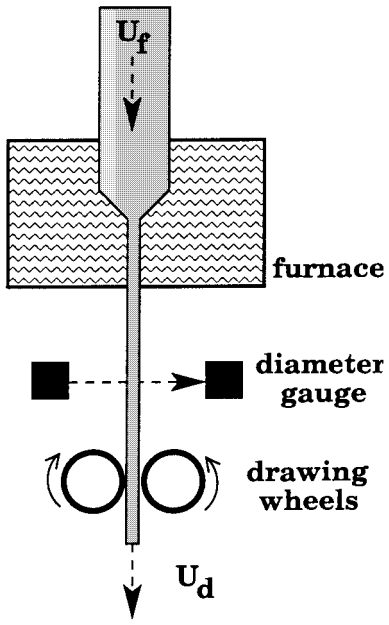

Figure 4. Experimental drawing apparatus - schematic.

find that, for the lower of the two temperatures, this has the value 1·15. This is order unity and so some control might be expected to be possible and the fact that no explosion or collapse took place during the experiment is consistent. For the higher of the two temperatures, however, we find that the the value of the sensitivity parameter is about $S = 18$. The conclusions of Section 4.6, namely that this should lead to severe sensitivity, are well confirmed when we observe from the lower pictures in Figure 3 that there seems to be only a fraction of a p.s.i. separating conditions that cause either complete collapse and explosion.

6.1. THEORY/EXPERIMENTAL COMPARISON FOR CAPILLARY SIZE

Some further experiments were then carried out with the aim allowing a more detailed and quantitative comparison with the theory. For these experiments, the silica capillary preform used had an OD of 28mm and an ID of 24mm. The glass used was Suprasil F300, a commercially-available high-quality low-impurity grade of silica commonly used for the production of low-loss optical fibres. Results from these experiments were described in more detail in [32], and are reviewed here for completeness.

A graphite furnace was used to heat the preform in a commercially-available 5m fibre Heathway drawing tower. The heating took place over a 3cm “hot zone”. For the purposes of comparison, we will assume that a constant temperature was maintained throughout this hot zone. The preform, whose top end was open to the atmosphere so that no internal hole pressurisation was present, was fed into the furnace at a constant feed speed and the final diameter of the drawn capillary was measured using a laser diameter gauge positioned approximately 1m below the furnace. The draw speed was controlled by passing the drawn capillaries through a pair of wheels rotating at a set speed whose surface is designed to avoid slippage. A schematic of the drawing arrangement is given in Figure 4.

A total of 24 experimental runs were carried out, during which the feed speed was varied between 2 and 8 mm/min and the draw speed between 0·6 to 1·2m/min. Furnace temperatures

of 1900, 1950 and 2000 °C were used. Once any particular combination of drawing conditions was set, the process was allowed to stabilise before the final dimensions of the drawn capillary were measured. Because the distance between the drawing wheels and the neck-down region was relatively large, the system took less time to stabilise at lower temperatures as a result of the rapid increase of viscosity with reduced temperature. After drawing, the OD of each capillary was measured both using the diameter gauge and a micrometer. The final IDs were extracted from measurements made using a standard optical microscope. The law of mass conservation provided an extra check on the validity of the ID measurements; this requires that, in steady state, the feed and draw volume fluxes should be equal. The experimental results exhibited only small deviations from this requirement, with a maximum error in volume flux of just over 5%; however, the error was less than 2% for the majority of the experiments. This indicates not only that the final capillary dimensions have been measured accurately, but also that sufficient time has been allowed for the process to stabilise.

After completion of the experimental programme, a comparison was made with the theoretical predictions of (35) and (36). For comparison purposes, we set $x = L = 3$cm in (36) and used the known experimental values for U_f, U_d, h_{10} and h_{20}. The remaining required piece of information, namely the ratios γ/μ at the furnace operating temperatures, does not appear to be available for Suprasil F300. It is also the case that, while the three drawing temperatures are likely to be accurate relative to each other, it is possible that they may suffer from an absolute temperature offset by as much as 50 °C. For each furnace temperature, we therefore fitted the theoretical model to the experimental data by choosing the parameter γ/μ; the relevant values for 1900 °, 1950 °C and 2000 °C were $1{\cdot}61 \times 10^{-6}$m/sec, $3{\cdot}85 \times 10^{-6}$m/sec and $1{\cdot}12 \times 10^{-5}$m/sec, respectively.

The final measured outer diameters of the drawn capillaries are shown (symbols) as a function of the draw speed U_d in Figure 5. The theoretical predictions from (36) are indicated by lines. The corresponding results for the inner capillary diameters are shown in Figure 6. In each case, the comparison between the theory and the experimental results is striking, suggesting that the theoretical model is a powerful predictive tool for capillary drawing.

Not surprisingly, higher temperatures, smaller feed speeds or larger draw speeds all lead to smaller final capillary dimensions. Note that at larger feed speeds the final dimensions are more sensitive to the draw speed than at smaller feed speeds. For the range of experimental conditions considered here, the degree of capillary collapse is relatively small in each case. (In the most extreme case the final ID/OD ratio was 0·74, compared to its initial value of $24/28 \sim 0{\cdot}857$.) Further analysis of the data reveals that the degree of collapse is a strong function of feed speed, with the greatest amount of collapse occurring at the lowest feed speed, but is insensitive to draw speed.

7. Conclusions and discussion

In the above study we have been able to use asymptotic analysis to propose leading-order equations for the drawing of a capillary, the process that provides the raw material for holey fibres. This may be regarded as the first step towards a complete quantification of the process of drawing arbitrarily-shaped holey fibres. We have shown that our model gives excellent agreement with a range of experimental data, which gives us confidence in its powers as a predictive tool. As well as predictions in the form of data, however, it also provides some practical guidelines useful in the design and control of the manufacture of capillaries.

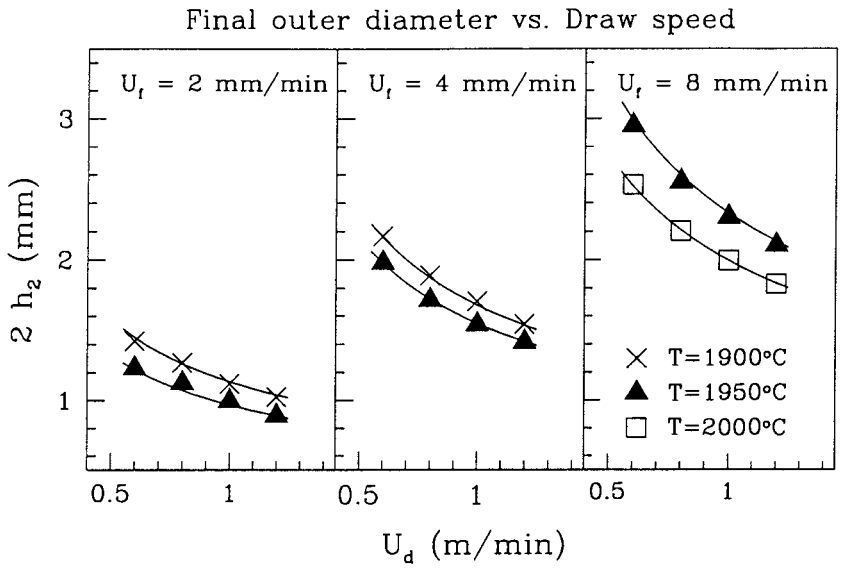

Figure 5. Experimental results (symbols) and theoretical predictions using (36) (lines) for capillary outer diameters.

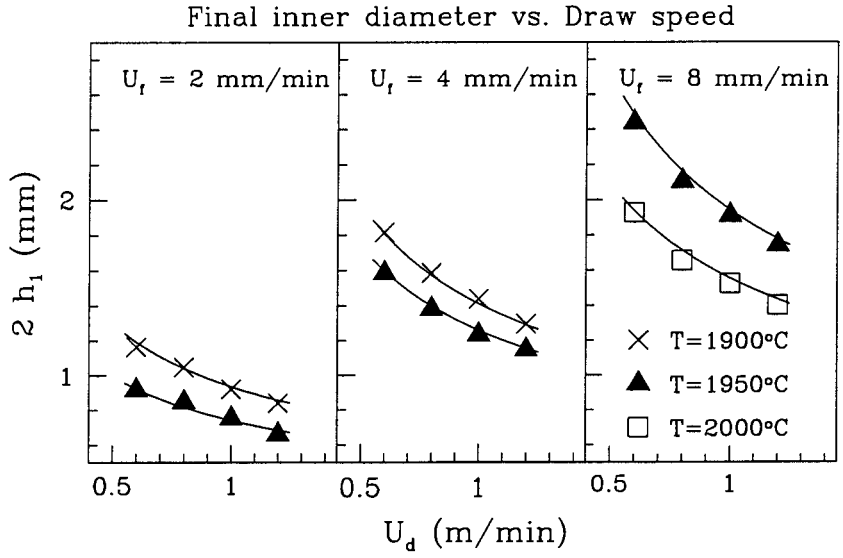

Figure 6. Experimental results (symbols) and theoretical predictions using (36) (lines) for capillary inner diameters.

It would be useful ultimately to be able to predict the drawing process for microstructured fibres with arbitrary cross-sectional profiles. The asymptotic techniques outlined above signpost a route forward for accomplishing this. Of course, other techniques such as homogenisation could also be used to relate results for capillaries to to those for more complicated, but regular structures.

Another way in which the model could be refined would be to include a more detailed model of the temperature and heating effects during the process of drawing. Bearing in mind the number of complicated transport processes that are involved and the difficulties of quan-

tifying them, however, this is likely to prove difficult. The model developed above allows the inclusion of a known furnace temperature profile, and this is a relatively simple parameter to measure.

It is worth making the point that detailed and rigorous comparison of the theory with experimental results is greatly complicated by the lack of suitable data regarding the surface tension and viscosity of glass. Although well-fitting formulae are available for the viscosity of the more common glasses as a function of temperature (see, for example [33, Chapter 6]) there seems to be a general dearth of such data for higher-quality glasses, perhaps because such information is regarded as being proprietary. It may prove difficult to test the theory severely if such values never become available, though one valuable use of models such as the one developed above is to independently determine crucial parameters such as these.

Acknowledgements

TMM and DJR acknowledge the support of Royal Society University Research Fellowships. The authors also thank Neil Broderick and Adam Wheeler for useful discussions and Peter Bennett for experimental assistance.

References

1. T.A. Birks, J.C. Knight and P. St. J. Russell, Endlessly single-mode photonic crystal fibre. *Opt. Lett.* 22 (1997) 961–963.
2. T.M. Monro, D.J. Richardson and P.J. Bennett, Developing holey fibres for evanescent field devices. *Elect. Lett.* 35 (1999) 1188–1189.
3. T.M. Monro, D.J. Richardson, N.G.R. Broderick and P.J. Bennett, Holey fibres: an efficient modal model. *J. Lightwave Technol.* 17 (1999) 1093–1102.
4. J.K. Ranka, R.S. Windeler and A. Stentz, Optical properties of high-delta air-silica microstructure optical fibres. *Opt. Lett.* 25 (2000) 796–798.
5. J.C. Knight, J. Broeng, T.A. Birks and P. St. J. Russell, Photonic band gap guidance in optical fibres. *Science* 282 (1998) 1476–1478.
6. M. Key, I.G. Hughes, W. Rooijakkers, B.E. Sauer, E.A. Hinds, D.J. Richardson and P.G. Kazansky, Propagation of cold atoms along a miniature magnetic guide. *Phys. Rev. Lett.* 84 (2000) 1371–1373.
7. M.R. Matovich and J.R.A. Pearson, Spinning a molten threadline – Steady-state isothermal viscous flows. *Ind. Eng. Chem. Fundam.* 8 (1969) 512–520.
8. J.R.A. Pearson and M.A. Matovich, Spinning a molten threadline - Stability. *Ind. Eng. Chem. Fundam.* 8 (1969) 605–609.
9. Y.T. Shah and J.R.A. Pearson, On the stability of nonisothermal fiber spinning. *Ind. Eng. Chem. Fundam.* 11 (1972) 145–149.
10. Y.T. Shah and J.R.A. Pearson, On the stability of nonisothermal fiber spinning - general case. *Ind. Eng. Chem. Fundam.* 11 (1972) 150–153.
11. J.A. Burgman, Liquid glass jets in the forming of continuous fibers. *Glass Technol.* 11 (1970) 110–116.
12. L.R. Glicksmann, The cooling of optical fibres. *Glass Technol.* 9 (1968) 131–138.
13. G. Manfre, Forces acting in the continuous drawing of glass fibres. *Glass Technol.* 10 (1969) 99–106.
14. F.T. Geyling and G.M. Homsy, Extensional instabilities of the glass fiber drawing process. *Glass Technol.* 21 (1980) 95–102.
15. F.T. Geyling, Basic fluid dynamic considerations in the drawing of optical fibres. *Bell Sys. Tech. J.* 55 (1976) 1011–1056.
16. J.N. Dewynne, P.D. Howell and P. Wilmott, Slender viscous fibres with inertia and gravity. *Quart. J. Mech. Appl. Math.* 47 (1994) 541–555.
17. J.N. Dewynne, J.R. Ockendon and P. Wilmott, On a mathematical model for fibre tapering. *SIAM J. Appl. Math.* 49 (1989) 983–990.

18. H. Papamichael and I.N. Miaoulis, Thermal behavior of optical fibres during the cooling stage of the drawing process. *J. Mater. Res.* 6 (1991) 159–167.
19. S.E. Rosenberg, H. Papamichael and I.N. Miaoulis, A two-dimensional analysis of the viscous problem of a glass preform during the optical fiber drawing process. *Glass Technol*. 35 (1994) 260–264.
20. Z. Yin and Y. Jaluria, Thermal transport and flow in high-speed optical fiber drawing. *J. Heat Transfer, Trans ASME* 120 (1998) 916–930.
21. P. Gospodinov and A.L. Yarin, Draw resonance of optical microcapillaries in non-isothermal drawing. *Int. J. Multiphase Flow* 23 (1997) 967–976.
22. A.L. Yarin, P. Gospodinov and V.I. Roussinov, Stability loss and sensitivity in hollow fiber drawing. *Phys. Fluids* 6 (1994) 1454–1463.
23. S.D. Sarboh, S.A. Milinkovic and D.L.J. Debeljkovic, Mathematical model of the glass capillary tube drawing process. *Glass Technol.* 39 (1998) 53–67.
24. M. Hucker, I. Bond, A.-A. Foreman and J. Hudd, Optimisation of hollow glass fibers and their composites. *Adv. Composite Lett.* 8 (1999) 181–189.
25. S. H-K. Lee and Y. Jaluria, Simulation of the transport processes in the neck-down region of a furnace drawn optical fibre. *Int. J. Heat Mass Transfer* 40 (1997) 843–856.
26. U.C. Paek and R.B. Runk, Physical behaviour of the neck-down region during furnace drawing of silica fibers. *J. Appl. Phys.* 49 (1978) 4417–4422.
27. N.P. Bansal and R.H. Doremus, *Handbook of Glass Properties*. New York: Academic Press (1986) 680pp.
28. W.W. Schultz and S.H. Davis, Effects of boundary conditions on the stability of slender viscous fibers. *Trans. ASME, J. Appl. Mech.* 51 (1984) 1–5.
29. G. Hall and J.M. Watt (eds), *Numerical Methods for Ordinary Differential Equations*. Oxford: Clarendon Press (1976) 336pp.
30. D. Gelder, The stability of the fiber drawing processes. *Ind. Eng. Chem. Fund.* 10 (1971) 534–535.
31. J.C. Chang, M.M. Denn and F.T. Geyling, Effects of inertia, surface tension and gravity on the stability of isothermal drawing of Newtonian fluids. *Ind. Eng. Chem. Fund.* 20 (1981) 147–149.
32. A.D. Fitt, K. Furusawa, T.M. Monro and C.P. Please, Modeling the Fabrication of Hollow Fibers: Capillary Drawing. *J. Lightwave Technol.* 19 (2001) 1924–1931.
33. R.H. Doremus, *Glass Science*. New York: Wiley Interscience (1973) 349pp.